Open access • Journal Article • DOI:10.1061/(ASCE)1090-0241(1997)123:9(818)

Settlement of reinforced sand in foundations

Nainan P. Kurian, K. S. Beena, R. Krishna Kumar

Published on: 01 Sep 1997 - Journal of Geotechnical and Geoenvironmental Engineering (American Society of Civil Engineers)

Topics: Bearing capacity, Settlement (structural), Foundation (engineering) and Mechanically stabilized earth

SETTLEMENT OF REINFORCED SAND IN FOUNDATIONS

By Nainan P. Kurian,[1] K. S. Beena,[2] and R. Krishna Kumar[3]

ABSTRACT: The technique of reinforcing soil for foundation improvement is well established. This paper addresses the aspect of settlement of reinforced sand foundations, where the major part of the existing work deals with the aspect of bearing capacity. A detailed analysis is made paying individual attention to soil, reinforcement, and the interface between the two. A three-dimensional, nonlinear finite-element analysis is presented that uses a three-dimensional, nonlinear soil-reinforcement interface friction element, along with other three-dimensional elements to model the system. The results of the analysis are compared with those from tests conducted in the laboratory and are found to be in good agreement. The studies lead to a better understanding of the behavior of the system at different stages of loading.

INTRODUCTION

The technique of reinforcing soil, which in its present form owes its origin to Vidal (1969), is one of the more recent and fast-growing techniques of soil improvement in the field of geotechnical engineering. The early structures built using this technique were earth retaining structures, but it was eventually realized that the technique is also useful in foundation problems. The method of reinforcing soil with layers of individual reinforcements placed horizontally as described here is best attempted in conjunction with fills that are required to support shallow foundations such as footings.

The first significant study on its use in foundations was by Binquet and Lee (1975), who concluded that the bearing capacity of sand increases as much as three times, sometimes even more, with a moderate amount of reinforcement in the form of aluminum strips. They also proposed a theoretical solution for obtaining the factor of safety against bearing capacity failure, based on their experimental studies. Akinmusura and Akinbolade (1981) studied the bearing capacity of a square footing supported by sand that was reinforced by natural fibers like iko. Reinforced earth slabs have been studied by Fragaszy and Lawton (1984) with a strip footing on sand reinforced by aluminum foil placed in several layers.

Studies have been carried out by Kinney (1982) to evaluate the effects of geotextiles placed at the interface between a soft clay and fine crushed gravel by conducting model tests. Singh (1988) has reported an extensive program of studies involving tests and analysis of reinforced soil beds.

Most of the aforementioned studies deal with the aspect of bearing capacity, whereas in the majority of cases, the design of shallow foundations in sand is governed by settlement rather than bearing capacity (Kurian 1992). Thus settlement-based design has been the prime motivating factor behind the present studies. Only very limited information is available in the literature [e.g., Nagoa et al. (1988) and Gens et al. (1989)] on the settlement of reinforced sand beds, especially in three-dimensional (3D) situations, which is necessary in the case of problems such as isolated footings.

The fast pace in the use of computers constantly extends the domain of the application of the finite-element method (FEM). FEM has indeed become a highly useful tool for the numerical analysis of problems such as the present one involving soil and reinforcement. Analysis of reinforced soil beds requires special treatment since the most important and yet the least known parameter in working with reinforced soil is the shear bonding capacity describing the soil-reinforcement interface behavior, as commented by Lee (1978) in his state-of-the-art report to the first "Soil-Reinforcement Conference" held in Pittsburgh. An early approach to considering reinforced soil has been based on the "unit cell" approach (Romstad et al. 1976), which introduces the effect of reinforcement in the constitutive law of the soil matrix by homogenization methods. This approach may be appropriate only when there are numerous reinforcing elements that enable the soil-reinforcement matrix to be considered as an essentially homogeneous material and where the opportunities of the integral mass can be determined. However, in many cases like those described in this paper, the reinforcement elements and the interface behavior need explicit modeling if the aim is to obtain more realistic results.

In this paper, a 3D finite-element analysis is presented giving individual attention to soil, reinforcement, and their interface, and the results have been compared with those from model tests conducted in the laboratory. Based on the joint element developed by Goodman et al. (1968) a 3D soil-reinforcement interface friction element has been developed, which is used along with other 3D elements in this analysis. The details of this formulation are given in Appendix I.

NUMERICAL IMPLEMENTATION

The interface element, described in Appendix I, is implemented with a general purpose finite-element program that is capable of modeling the nonlinear elastic behavior of the soil. An existing 3D isoparametric, eight-noded brick element is used to represent the soil medium, and a 3D truss element is used to model the reinforcement (Zienkiewicz 1977; Desai and Abel 1972). Both the reinforcement and the interface elements are geometrically 3D line elements. However they are physically characterized by the cross-sectional areas in the case of the truss element and the width of the contact (along the y-direction) between the reinforcement and the soil medium in the case of the interface element. For a reinforcement such as coir rope (rope made of fibers from the husk of coconut), this width is taken as its average diameter. Since the aim has been to develop a general 3D interface element, taking the width of the interface into account in the described manner enables the convenient modeling of the interfaces of reinforcements of different shapes such as bars, strips, and flats. The stress-strain behavior of soil is approximated by a hyperbolic relationship, following Duncan and Chang (1970). Incremental or piecewise linear method (Desai and Abel 1972) is used for the analysis in which the load is divided into a number of increments and

[1]Prof. of Geotech. Engrg., Dept. of Civ. Engrg., Indian Inst. of Technol., Madras, Madras—600 036, India.

[2]Asst. Dir., Irrig. Des. and Res. Board, Vikas Bhavan, Thiruvananthapuram—695 033, Kerala, India.

[3]Asst. Prof., Dept. of Mech. Engrg., Indian Inst. of Technol., Madras, Madras—600 036, India.

Note. Discussion open until February 1, 1998. To extend the closing date one month, a written request must be filed with the ASCE Manager of Journals. The manuscript for this paper was submitted for review and possible publication on June 18, 1996. This paper is part of the ***Journal of Geotechnical and Geoenvironmental Engineering***, Vol. 123, No. 9, September, 1997. ©ASCE, ISSN 1090-0241/97/0009-0818–0827/$4.00 + $.50 per page. Paper No. 8318.

J. Geotech. Geoenviron. Eng. 1997.123:818-827.

the [C] matrix (constitutive matrix) is updated for each increment in the analysis. The initial stresses are input based on the assumed at-rest values.

In a similar manner as the soil, interface properties are also treated as nonlinear, following the hyperbolic relationship (Desai 1974). The assigning of width to the interface, together with the 3D behavior of the system, necessitates the consideration of k_{s2} (the shear stiffness along the width, i.e., the y-direction). In the analysis k_{s2} is taken as equal to k_{s1} for convenience, and the normal stiffness k_n is given an absolute high value to prevent interpenetration of nodes. k_{s1} is allowed to vary hyperbolically, depending on the stress condition, as shown in the following (Desai 1974):

$$k_{st} = \left[1 - \frac{R_f' \tau}{c_a + \sigma_n \tan \delta}\right]^2 K' \gamma_w \left[\frac{\sigma_n}{P_a}\right]^{n'} \quad (1)$$

During loading, if a soil element is found to fail in shear, the same is noted, but no changes are effected, and the element is allowed to follow the hyperbolic relation as before, in keeping with the nonlinear elastic formulation of the problem. However, as regards the elements that fail in tension, the same are assigned a very small value of E for the subsequent loads. If during loading, the interface fails in shear (slip), the value of shear stiffness in the element is reduced to a small value; if tensile condition (debonding) develops across the interface elements, both shear and normal stresses are assigned small values, as per the usual practice followed in this regard.

APPLICATION

Details of Laboratory Investigations

Model tests were conducted on a sand bed prepared in a tank of dimensions 1.6 × 1.6 × 0.75 m, using a steel footing of dimensions 200 × 200 × 18 mm (Beena 1986; Ayyar et al. 1988). The soil used was uniformly graded sea sand, with properties $G = 2.72$, $D_{10} = 0.23$ mm, $C_u = 1.34$, $e_{min} = 0.51$, and $e_{max} = 0.72$.

The sand was filled in layers of 100-mm thickness (except the bottommost layer, which was 150 mm) to a total depth of 750 mm, compacting each layer by a falling-weight assembly to get a relative density of 0.5.

After conducting a reference test on unreinforced sand, reinforcements were introduced at appropriate levels, as per the schematic shown in Fig. 1. The reinforcing material used was coir rope 4.3-mm in diameter tied to bamboo strips of size 35 × 5 mm, which served as anchorages. Two additional bamboo strips were placed between the anchor strips near the edges to keep the ropes straight at the beginning of the test. The reinforcement pattern used was such that the reinforcements in one layer were perpendicular to the reinforcements in the layer immediately above or below. Four layers of reinforcements were placed at a vertical spacing of 100 mm. The horizontal spacing(s) and length of coir rope (L) varied from case to case. The loads were applied in small increments, measuring the settlements at each stage and using dial gauges placed at the top of the footing, at the center, and at the corners.

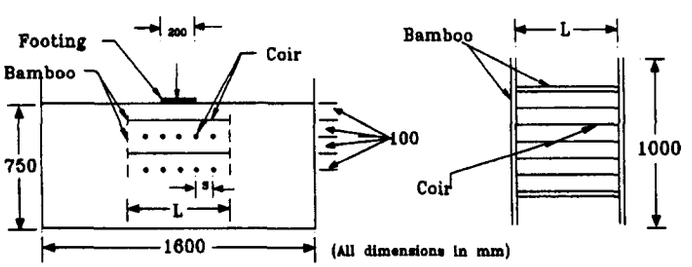

FIG. 1. Schematic of Test Setup

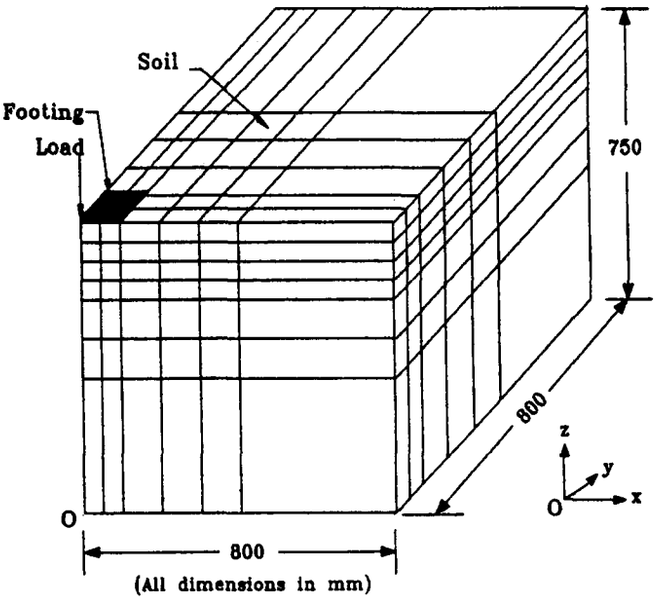

FIG. 2. Finite-Element Mesh

Finite-Element Mesh

The finite-element mesh used for the analysis of the system, shown in Fig. 2, was finalized after conducting necessary convergence studies using different meshes. The unreinforced case and five typical reinforced cases have been selected for finite-element modeling and analysis. Since the same mesh finalized as in the preceding is used to analyze different cases, the configuration and numbering of the mesh is done considering all the cases. The mesh consisted of 256 brick elements with 904 nodes. The number of truss elements and the interface elements varied with each case. As regards the soil-interface–reinforcement connectivity, one edge of the interface element (1-2 or 3-4) is attached to the soil and the other to the reinforcement. Before loading, 1 and 4 as well 2 and 3 coincide with each other. Fig. 3 shows the details of the connection between the reinforcement and the interfaces.

Material Properties

For the analysis, the footing and the reinforcements are treated as linearly elastic, defined by the elastic modulus (E) and the Poisson's ratio (μ). Nonlinear elastic behavior of the soil is represented by the tangent modulus E_t, defined by the hyperbolic formula (Desai and Abel 1972)

$$E_t = \left[1 - \frac{R_f(1 - \sin \phi)(\sigma_1 - \sigma_3)}{2c \cos \phi + 2\sigma_3 \sin \phi}\right]^2 KP_a \left[\frac{\sigma_3}{P_a}\right]^n \quad (2)$$

Laboratory Determination of the Hyperbolic Constants

Triaxial tests were conducted on representative samples of soil at various confining pressures to determine the hyperbolic constants K, n, and R_f. The results were plotted on a transformed axis to get a and b in the hyperbolic equation proposed by Kondner and Zelasko (1963), in which $(\sigma_1 - \sigma_3) = \varepsilon/(a + b\varepsilon)$. Here a is the reciprocal of the initial tangent modulus, and b is the reciprocal of the asymptotic value of the deviator stress $(\sigma_1 - \sigma_3)_{ult}$, obtained when the stress-strain curve approaches infinite strain. This value of $(\sigma_1 - \sigma_3)$ is related to the compressive strength [actual strength obtained from tests = $(\sigma_1 - \sigma_3)_f$] by a factor R_f, known as "failure ratio," such that $(\sigma_1 - \sigma_3)_f = R_f(\sigma_1 - \sigma_3)_{ult}$. Knowing $(\sigma_1 - \sigma_3)_{ult}$ and $(\sigma_1 - \sigma_3)_f$, R_f can be obtained from preceding relation. The other

J. Geotech. Geoenviron. Eng. 1997.123:818-827.

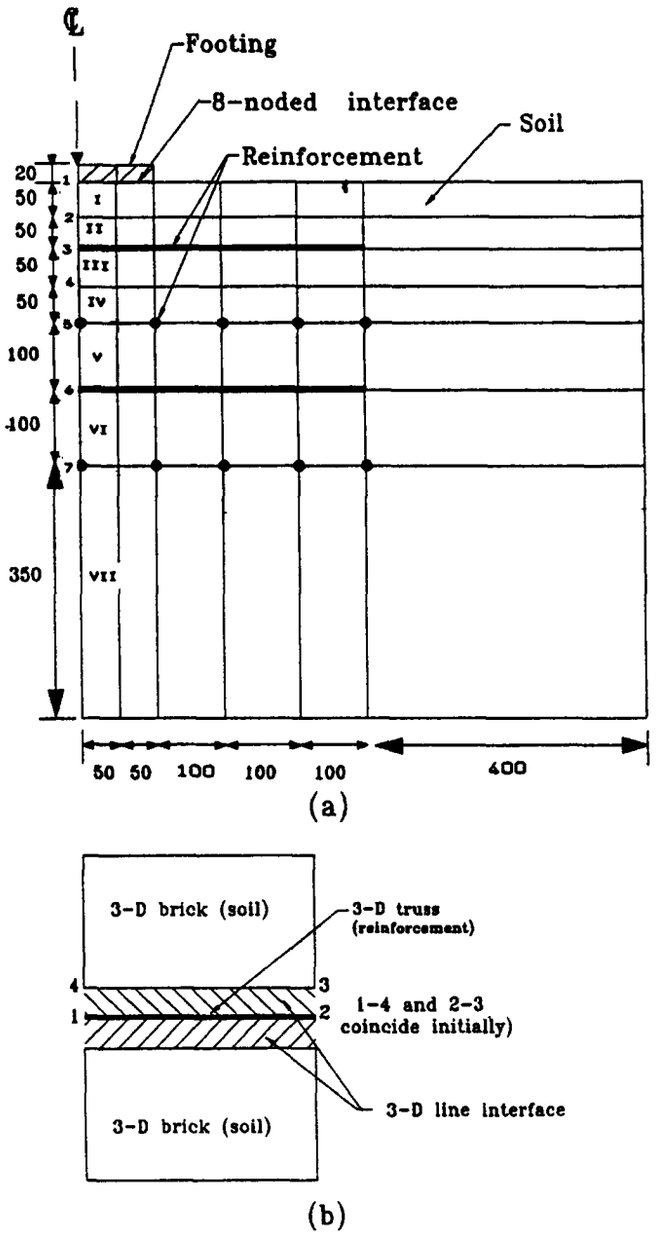

FIG. 3. Finite-Element Modeling of Reinforced Sand: (a) Central Section; (b) Soil-Reinforcement Interface

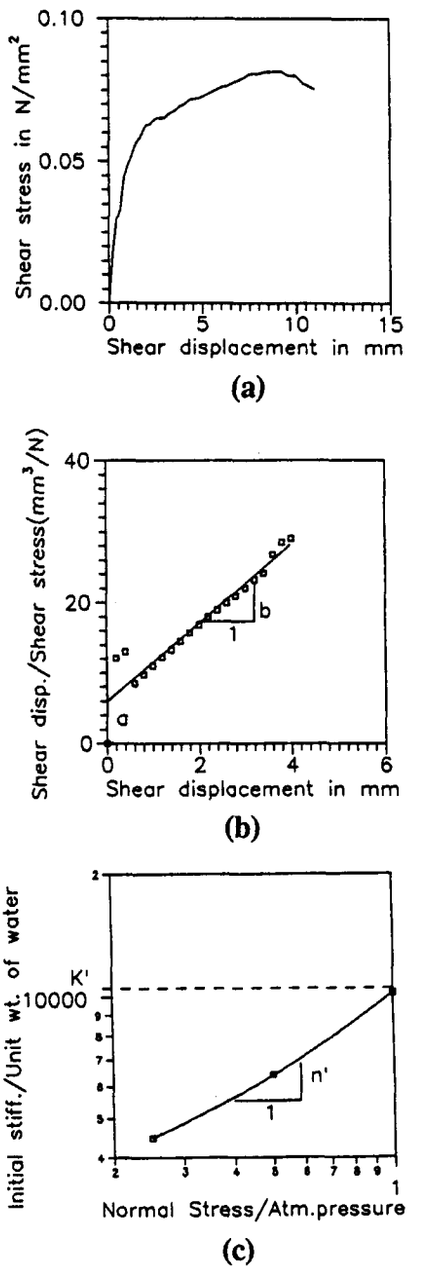

FIG. 4. Determination of Hyperbolic Constants for Interface

hyperbolic parameters, viz, K and n, are obtained by plotting E_i [i.e., $(1/a)$] and (σ_3/P_a) to log-log scales and fitting a straight line. n is the slope of this straight line and K is the ordinate at unit value on the x-axis.

In a similar manner as the soil, the hyperbolic parameters R_f', K', and n' for different interfaces (sand-steel, sand-coir, and sand-bamboo) are obtained by conducting direct shear tests. The bottom half of the shear box was fitted with the reinforcing material and the top half filled with the representative soil. In the case of sand-steel interface, the bottom half of the direct shear box was fitted with a steel block specimen. In the other two cases, the interfaces were produced by gluing the corresponding material on a wooden block in such a manner that the top surface exactly coincides with the surface of sliding. (In the case of coir, the surface of sliding coincided with the horizontal diameters of the ropes.) The direct shear test, which is a sliding test, was utilized instead of the pullout test, since the medium sand in the tests is assumed to slide laterally over the reinforcement when loaded vertically. Shear stress (τ) versus shear deformation (Δ) is plotted at a given value of σ_n, and τ_{max} is obtained. In this case the hyperbolic relation is obtained by the expression $\tau = \Delta/(a' + b'\Delta)$. A transformed plot is used to determine a' and b' as in the case of soil. R_f' is obtained by using τ_{max} and $1/b$. The test is repeated for different normal stresses. A log-log plot is drawn to get K' and n', as shown in Fig. 4.

The values of the material properties and the hyperbolic constants are obtained prior to the testing of the reinforced soil system and used in its analysis, which is tabulated in Appendix II. The same makes it a case of "blind" (noniterative) prediction.

Loading

Load increments are given simulating the loading stages applied in the tests. In general, 14 increments are given from 1 kN to 9 kN. Closer intervals are used at higher loads to better

J. Geotech. Geoenviron. Eng. 1997.123:818-827.

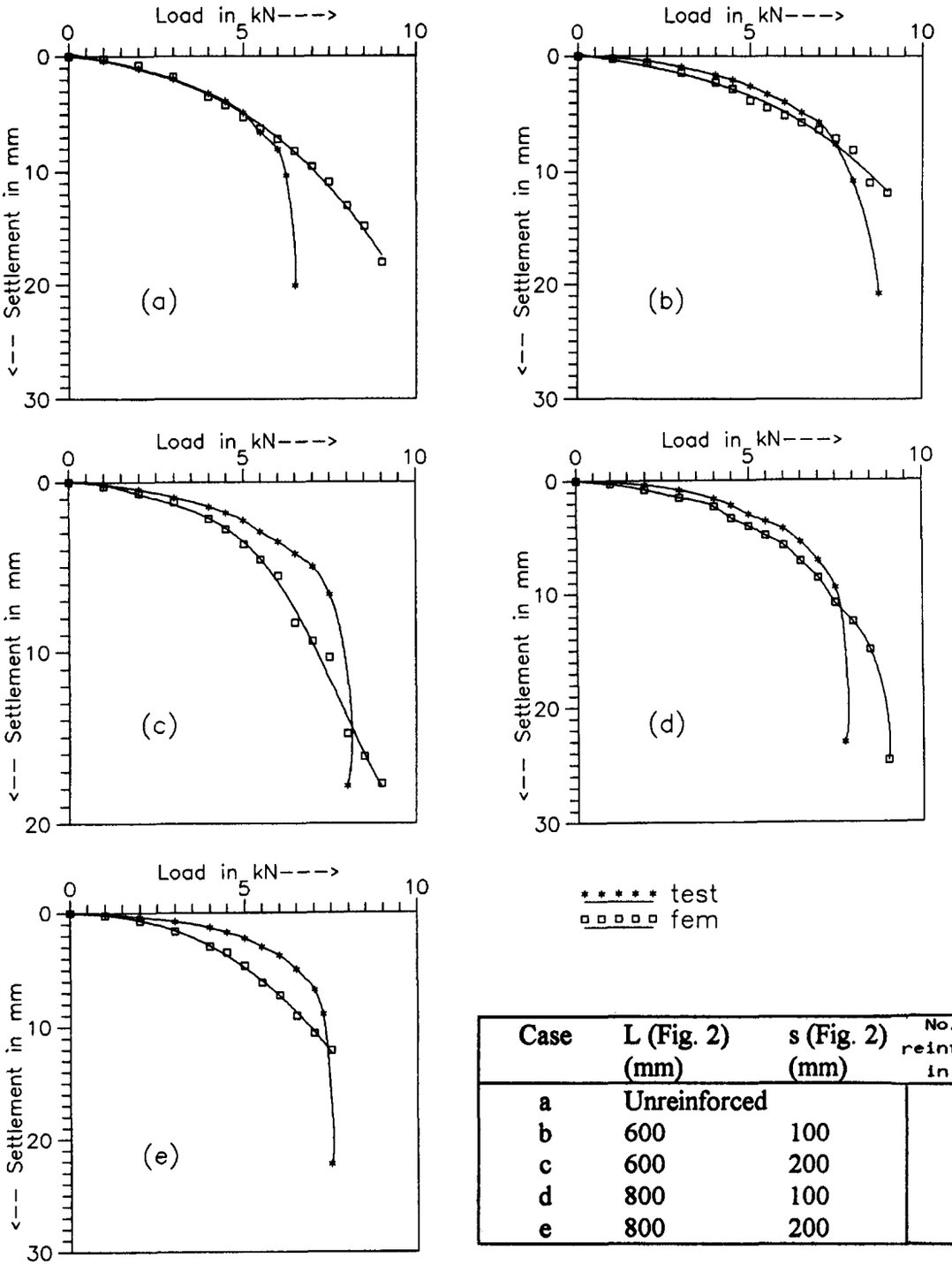

Case	L (Fig. 2) (mm)	s (Fig. 2) (mm)	No. of coir reinforcements in a layer
a	Unreinforced		
b	600	100	5
c	600	200	2
d	800	100	7
e	800	200	3

(f)

FIG. 5. Load-Settlement Diagrams

reflect the nonlinear response. The loads are applied as point loads on the axis of the footing.

RESULTS AND ANALYSIS

Load-Deformation Behavior

The load settlement behavior of the system at the top of the footing is shown in Fig. 5. The corresponding data are presented in Table 1. The settlements at all points on the footing at each load stage were uniform both in the test and the analysis. The load-settlement curves obtained from the tests and the finite-element analysis show good match, both for the unreinforced [Fig. 5(a)] and reinforced cases [Fig. 5(b–e)], particularly over the range of response significant from the practical point of view in design. The predicted responses are found to diverge from the experimental results only in the final range. The reason for this is that the analysis does not take into account the plasticity or the strain softening aspects. However, to the foundation engineer, the region of interest is the working load range, which is about one-third or at most one-half of the ultimate value, and in those regions the results of the analysis and the experiment show good agreement. Where difference exists, the numerical predictions are on the conservative side, except in the final range, in all the reinforced cases.

The difference in the initial stage can be due to the errors

J. Geotech. Geoenviron. Eng. 1997.123:818-827.

TABLE 1. Load versus Settlement: Experimental and Numerical Results

Load (kN) (1)	SETTLEMENT (mm)									
	Case a		Case b		Case c		Case d		Case e	
	Experimental (2)	Numerical (3)	Experimental (4)	Numerical (5)	Experimental (6)	Numerical (7)	Experimental (8)	Numerical (9)	Experimental (10)	Numerical (11)
0.0	0.00	0.00	0.00	0.00	0.00	0.00	0.00	0.00	0.00	0.00
1.0	0.43	0.38	0.08	0.32	0.21	0.34	0.12	0.53	0.10	0.32
2.0	1.02	0.97	0.42	0.65	0.48	0.72	0.78	1.09	0.48	0.66
3.0	1.98	1.81	1.02	1.37	1.01	1.18	1.02	1.84	0.97	1.58
4.0	3.07	3.37	1.63	2.30	1.57	2.16	1.91	2.18	1.21	2.97
4.5	3.92	4.26	2.01	2.98	1.98	2.71	2.21	3.82	1.89	3.71
5.0	4.87	5.16	2.57	3.78	2.26	3.67	3.04	4.21	2.21	4.72
5.5	6.48	6.08	3.31	4.28	3.01	4.74	3.89	5.16	3.02	6.16
6.0	7.96	7.01	3.98	4.91	3.52	5.66	4.17	5.92	3.92	7.10
6.5	19.82	8.16	4.82	5.53	4.19	8.23	5.76	7.22	5.00	9.01
7.0		9.32	5.60	6.21	5.21	9.62	7.18	8.57	7.02	10.68
7.5		10.71	7.46	7.02	6.87	10.51	9.36	11.12	22.17	12.18
8.0		13.02	10.61	8.03	17.82	14.87	23.42	12.41		
8.5		14.73	20.86	10.91		16.21		15.11		
9.0		18.06		11.78		17.89		24.81		

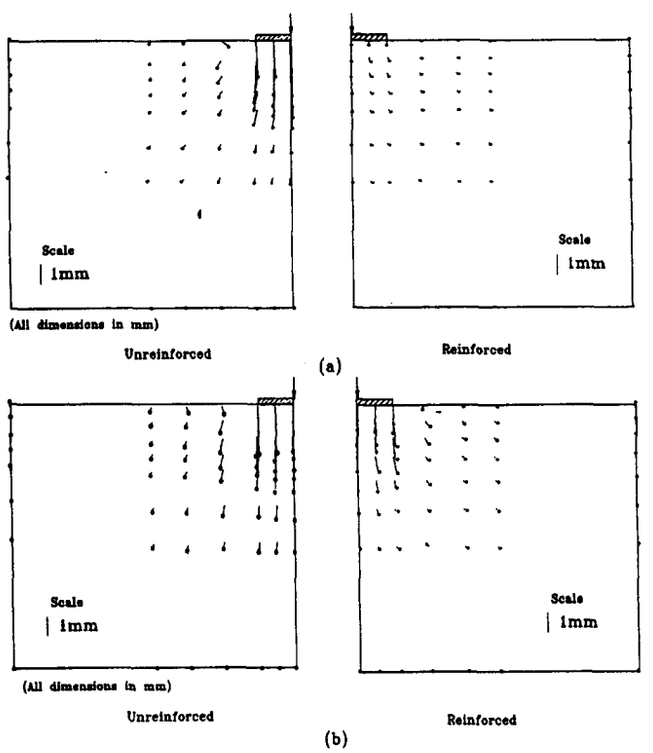

FIG. 6. Displacement Field Diagram at Loads of: (a) 1 kN; (b) 3 kN

associated with determining the material properties in the analysis, especially when only a representative sample is used for finding out the properties of the soil. Even a small error in determining the soil properties like K and n is found to affect the results considerably, especially in the initial stage of loading, making the numerical model a sensitive one. If more precise results are sought, it is possible to perform a parametric study from which the appropriate values of the material constants can be back-predicted and used in the subsequent analysis. However, as stated before, the present attempt has been a "blind" prediction and not a "calibrated" analysis.

The remaining results are presented and discussed with respect to the central symmetrical plane for the case in Fig. 5(b) only, which is considered as typical.

TABLE 2. Vertical Center Line Displacements

Node number (Fig. 3) (1)	SOIL DISPLACEMENT (mm)			
	Load: 1 kN		Load: 3 kN	
	Unreinforced (2)	Reinforced (3)	Unreinforced (4)	Reinforced (5)
1	0.378	0.321	1.811	1.371
2	0.331	0.248	1.358	1.068
3	0.283	0.189	0.914	0.767
4	0.239	0.143	0.608	0.518
5	0.204	0.096	0.312	0.272
6	0.178	0.072	0.187	0.197
7	0.157	0.048	0.143	0.073

Displacement Field

Fig. 6 shows the resultant displacement fields on the central X-Z plane for loads of 1 and 3 kN for both the unreinforced and reinforced cases. The dots shown correspond to the final displaced position of the respective vectors. The major component of displacement is in the downward vertical direction nearer the footing. The soil displacement along the axis of the footing is entered in Table 2. (There has been a small heave of the soil mass slightly away from the footing that could not be depicted to scale.) Comparing the unreinforced and reinforced cases, it is observed that there is a clear reduction of settlement in the reinforced cases at the higher loads. At the first stage of loading there is actually a small increase in settlement in the case of reinforced soil. This may be because the normal load may not be sufficient to develop enough friction between the soil and reinforcement, which is the major factor contributing to reduction in settlement. In other words, the reinforcements can initially behave as a plane of weakness that is overcome by the development of friction as the load increases. At any rate, at values of working loads, which are increased due to the increase in ultimate bearing capacity, the settlements in reinforced soil are decisively smaller than in the unreinforced soil.

Relative Deformation between Soil and Reinforcement

Fig. 7 shows the relative shear deformations at the reinforcement (coir) and interface nodes for loads of 1 and 3 kN on the central X-Z plane. It is seen that there is considerable relative movement between the soil and the reinforcement,

which increases with load. The same, however, decreases with the depth of the reinforcement and increases with load. The relative deformations also show a decreasing tendency at the outer end of the reinforcement, presumably due to the presence of bamboo strip anchorages to which they are tied.

The variation of interface shear stresses predicted by the FEM analysis along the length of the coir reinforcement on the central *X-Z* plane is shown in Fig. 8. The shear stress at the interface is maximum at a distance of nearly $0.5B$ from the center of the footing, where B is the width of the footing, i.e., nearly below the edge of the footing. The same decreases to a very low value near the edges. The interface stresses also increase with load and are higher at the top layers.

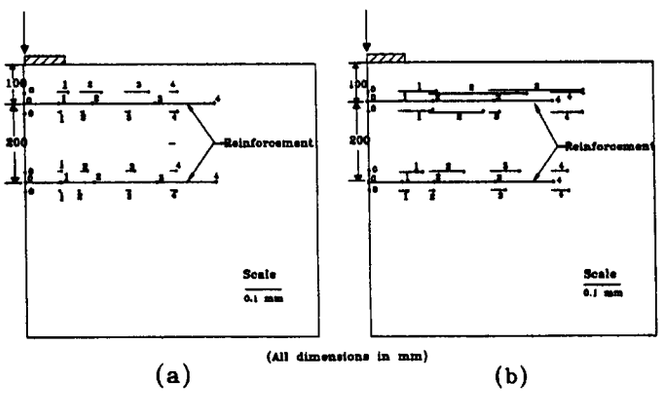

FIG. 7. Reinforcement-Interface Relative Deformations at Loads of: (a) 1 kN; (b) 3 kN

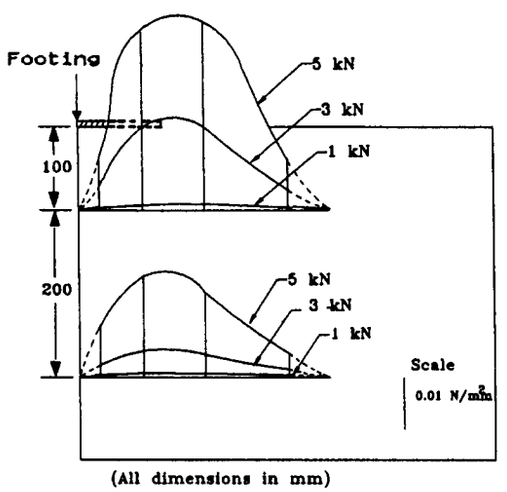

FIG. 8. Interface Shear Stresses

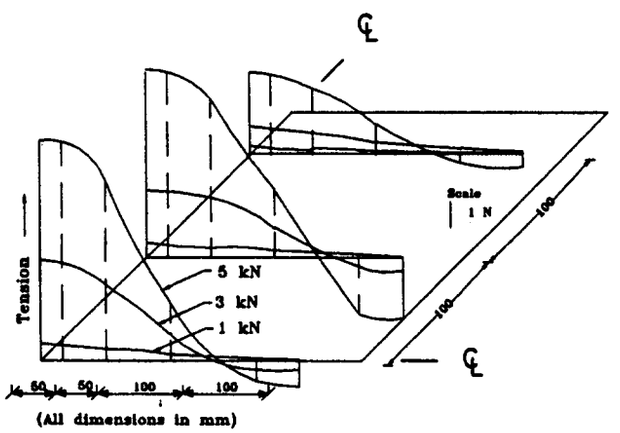

FIG. 9. Axial Force in Reinforcements

Axial Forces in Reinforcement

A typical variation of axial force in the coir reinforcements is shown in Fig. 9 for three values of loads. To get an isometric viewing effect, the axial forces along the reinforcements are plotted on tilted axes. It is seen from the figures that the maximum forces occur at points near the center and gradually reduce towards the end of the reinforcement. It has been observed in the study that the topmost reinforcement is subject to maximum stresses and the stresses developed decrease with depth, which shows that the reinforcement material is better utilized at the top layers. (The stresses developed in the bamboo anchorages also show the same trend.) As the load increases, the stress in the reinforcement increases faster, as we can see from the figures, indicating again that the reinforcement is more effective at higher loads. The compressive axial forces developing in coir are explained by their position (away from the center) and that they are anchored. In the case of no-compression reinforcements such as coir, iterative solutions are possible until the axial forces are either tensile or zero. The effect of axial compression—which is unrealistic in the present case—on the solution cannot, however, be predicted from the present analysis.

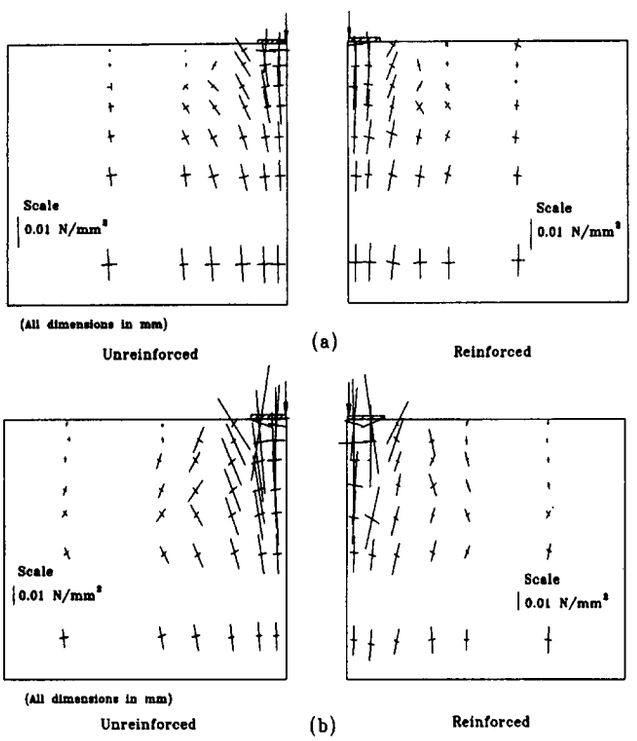

FIG. 10. Principal Stresses at Loads of: (a) 1 kN; (b) 3 kN

TABLE 3. Major Principal Stresses near Vertical Center Line

Element number (Fig. 3) (1)	PRINCIPAL STRESS (N/mm²)			
	Load: 1 kN		Load: 3 kN	
	Unreinforced (2)	Reinforced (3)	Unreinforced (4)	Reinforced (5)
I	0.034	0.033	0.063	0.062
II	0.026	0.030	0.058	0.061
III	0.021	0.026	0.051	0.058
IV	0.019	0.024	0.042	0.054
V	0.017	0.020	0.033	0.052
VI	0.013	0.016	0.020	0.031
VII	0.012	0.013	0.014	0.016

J. Geotech. Geoenviron. Eng. 1997.123:818-827.

Principal Stress Field

The principal stress fields for loads of 1 and 3 kN for the unreinforced and the reinforced cases are shown in Fig. 10. The major and minor principal stresses in their actual orientations are plotted at the centers of each element facing the central X-Z plane. The major principal stresses in the elements closest to the axis of the footing are entered in Table 3. As the load increases from 1 to 3 kN, the principal planes undergo a slight rotation below the center. The knowledge of orientation of principal stresses will be useful in determining more efficient orientations of the reinforcements.

Vertical Stress Contours

Fig. 11 shows the vertical stress (σ_z) contours at the central plane for a load of 3 kN, which corresponds to an applied stress of 0.075 N/mm^2. These are the stresses produced by the applied loads, determined by subtracting the initial stresses from the total stress obtained in the analysis. In general the contours are smooth in the unreinforced case, in contrast to which they show signs of stress concentration near the reinforcements in the reinforced case. The contours of the same stress are generally seen to shift downwards in the reinforced case, testifying to the strengthening of the soil brought about by the reinforcement in it.

Failure Progression

The finite-element analysis provides an interesting opportunity to trace the failure of the system, element by element, with load that is of considerable academic interest if not of practical value. Fig. 12 illustrates the failure developing in the soil elements adjacent to the central vertical plane. Failure can be in shear or in tension in the perpendicular direction. Fig.

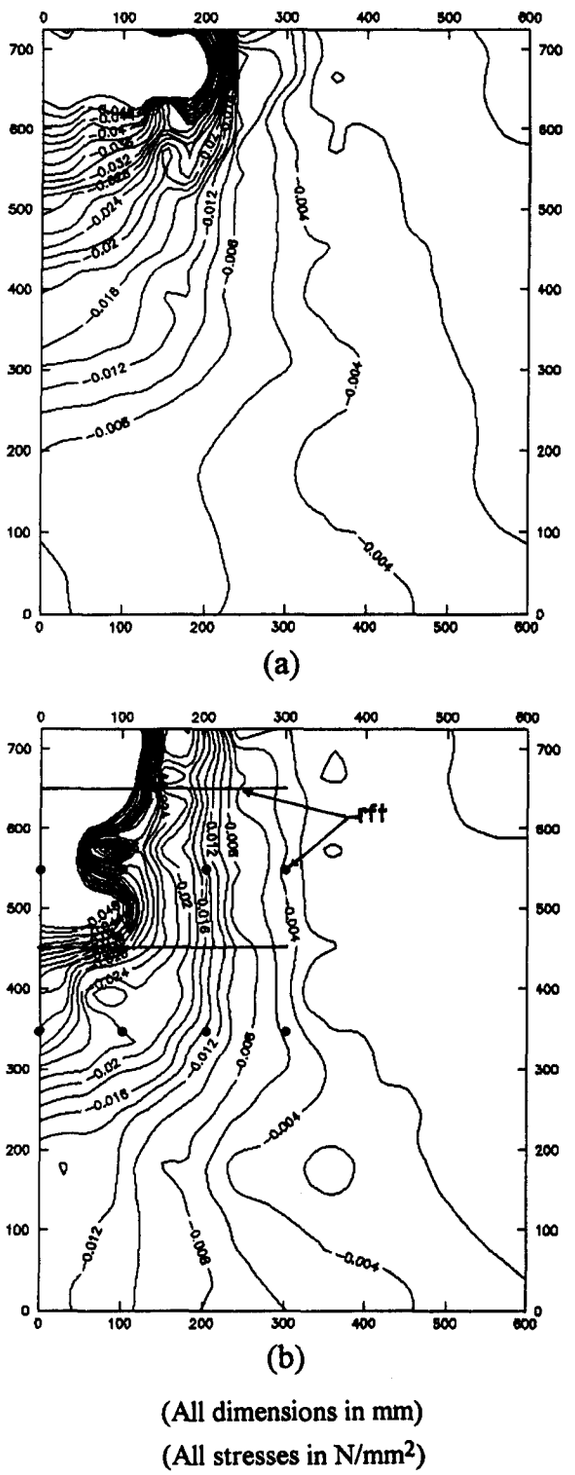

FIG. 11. Vertical Stress Contours due to Applied Load of 3 kN: (a) Unreinforced; (b) Reinforced

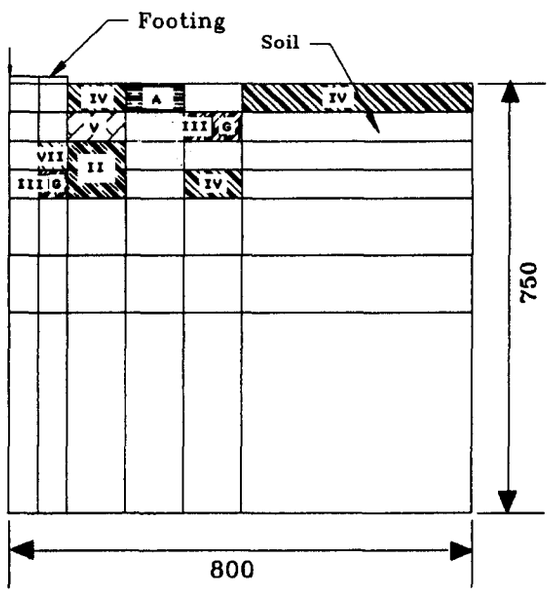

LEGEND

Increment No.	Load range(kN)	Failure in Shear	Failure in Tension
1	0.0–1.0	I	A
2	1.0–2.0	II	B
3	2.0–3.0	III	C
4	3.0–4.0	IV	D
5	4.0–4.5	V	E
6	4.5–5.0	VI	F
14	8.5–9.0	VII	G

FIG. 12. Progression of Failure of Soil Elements

J. Geotech. Geoenviron. Eng. 1997.123:818-827.

12 follows the legend given used for representing failure at various load stages. In examining this figure, it may be noted that some elements that fail at one stage "recoup" at a higher load stage and fail by a different mode at subsequent load stages. This explains the double entries found in some elements.

CONCLUSIONS

In this paper, for the detailed study of a reinforced soil system with layers of individual reinforcements placed horizontally under the footing, a 3D nonlinear finite-element analysis has been developed. With the help of a 3D line interface element, the frictional behavior of the soil-reinforcement interface is modeled in the analysis. The analysis accounts for the material nonlinearity of the soil, as well as that of the interface. The predicted results are compared with those from laboratory tests and are found to be in fair agreement, considering the sensitivity of the numerical model. The settlement of the reinforced soil system is found to be much less than that of the unreinforced soil, particularly at values close to working loads, which proves the effectiveness of the reinforcement in reducing settlement. The axial forces in the reinforcement are found to be maximum near the center, gradually reducing towards the end. The principal stresses at higher depths get reduced in the reinforced case. The stress contours shift downwards in the reinforced case, spreading the stresses deeper, thereby establishing the strengthening of the soil brought about by the reinforcements.

The method, even though expensive in terms of computing effort, gives complete information regarding deformations, stresses, and forces in the entire system at any stage of loading, which is extremely difficult, if not impossible, by any other method of analysis. Thus, it may be summarized that this detailed 3D finite-element analysis using interface elements leads to a better understanding of the overall behavior of reinforced soil systems under load, which enhances the level of confidence in constructing such soil structures for supporting foundations.

APPENDIX I. FINITE-ELEMENT FORMULATION OF FRICTIONAL SOIL-REINFORCEMENT INTERFACE ELEMENT

This special isoparametric element has been developed (Beena 1994) with a view to representing the friction (including adhesion) between soil and the reinforcement, especially when the reinforcements are in the form of rods or strips. Such reinforcements are not in contact with the whole surface of the soil mass at a particular level as in the case of a geotextile or a mat; if they were, one could have used the available eight-noded quadratic interface element for 3D analysis (Beer 1985; Muqtadir and Desai 1986). The geometry of the present element is such that it is a line with four nodes as shown in Fig. 13. A local coordinate system is chosen with the x-axis along the length and the origin at one end. The element has length L and zero thickness, as assumed by Goodman et al. (1968). A linear variation of displacement along the length of the element is assumed. Relative displacement between the top and bottom nodes is taken as the corresponding strain ε in the element (Goodman and St. John 1977).

Accordingly

$$\{\varepsilon\} = \begin{Bmatrix} \Delta u \\ \Delta v \\ \Delta w \end{Bmatrix} = \begin{bmatrix} u_{top} - u_{bot} \\ v_{top} - v_{bot} \\ w_{top} - w_{bot} \end{bmatrix} \tag{3}$$

where

$$u_{top} = N_{4u4} + N_{3u3}, \quad u_{bot} = N_{1u1} + N_{2u2} \tag{4a}$$

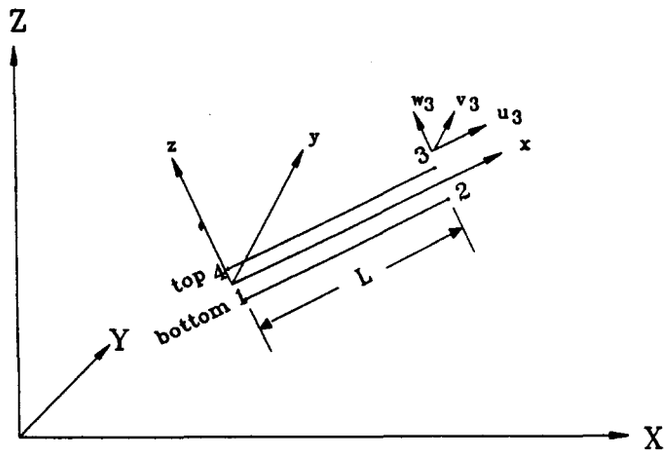

FIG. 13. Line Interface Element for 3D Analysis

$$v_{top} = N_{4v4} + N_{3v3}, \quad v_{bot} = N_{1v1} + N_{2v2} \tag{4b}$$

$$w_{top} = N_{4w4} + N_{3w3}, \quad w_{bot} = N_{1w1} + N_{2w2} \tag{4c}$$

in which N_1, N_2, etc. = corresponding shape functions. Also, $N_1 = N_4 = 1 - x/L$, and $N_2 = N_3 = x/L$.

From (3) and (4) we get

$$\{\varepsilon\} = \begin{bmatrix} -N_1 & 0 & 0 & -N_2 & 0 & 0 & N_2 & 0 & 0 & N_1 & 0 & 0 \\ 0 & -N_1 & 0 & 0 & -N_2 & 0 & 0 & N_2 & 0 & 0 & N_1 & 0 \\ 0 & 0 & -N_1 & 0 & 0 & -N_2 & 0 & 0 & N_2 & 0 & 0 & N_1 \end{bmatrix} \begin{Bmatrix} u_1 \\ v_1 \\ w_1 \\ \cdot \\ \cdot \\ \cdot \\ w_4 \end{Bmatrix} \tag{5}$$

from which the strain-displacement matrix

$$[B] = \begin{bmatrix} -N_1 & 0 & 0 & -N_2 & 0 & 0 & N_2 & 0 & 0 & N_1 & 0 & 0 \\ 0 & -N_1 & 0 & 0 & -N_2 & 0 & 0 & N_2 & 0 & 0 & N_1 & 0 \\ 0 & 0 & -N_1 & 0 & 0 & -N_2 & 0 & 0 & N_2 & 0 & 0 & N_1 \end{bmatrix} \tag{6}$$

and

$$u^T = \{u_1 \; v_1 \; w_1 \; u_2 \; v_2 \; w_2 \; u_3 \; v_3 \; w_3 \; u_4 \; v_4 \; w_4\} \tag{7}$$

From the principle of virtual work

$$\int_v \{\delta\varepsilon\}^T\{\sigma\}\, dv = \{\delta u\}^T\{F\} \tag{8}$$

In the present case it becomes

$$\int_0^L \{\delta\varepsilon\}^T\{\sigma\} b\, dx = \{\delta u\}^T\{F\} \tag{9}$$

Substituting for ε and σ, we get

$$\int_0^L \{\delta u\}^T[B]^T[C][B]\{u\} b\, dx = \{\delta u\}^T\{F\} \tag{10}$$

where b = width of the interface, which is the width of contact between soil and reinforcement along the y-direction. Rearranging the terms it becomes

$$\left[b \int_0^L [B]^T[C][B]\, dx \right] \{u\} = \{F\} \tag{11}$$

which is of the form $[k]\{u\} = \{F\}$.

From this the element stiffness matrix is obtained as

J. Geotech. Geoenviron. Eng. 1997.123:818-827.

$$[k] = b \int_0^L [B]^T [C][B]\, dx \tag{12}$$

The stress developed in the interface can be obtained as $[C]\{\varepsilon\}$, in which

$$[C] = \begin{bmatrix} k_{s1} & 0 & 0 \\ 0 & k_{s2} & 0 \\ 0 & 0 & k_n \end{bmatrix}$$

It may be noted that since the shearing and the normal displacements are uncoupled as in a nondilatant case (Ghaboussi et al. 1973), the $[C]$ matrix is left with no off-diagonal terms. From the preceding, the stress vector is obtained as

$$\begin{Bmatrix} \tau_x \\ \tau_y \\ \sigma_n \end{Bmatrix} = \begin{bmatrix} k_{s1} & 0 & 0 \\ 0 & k_{s2} & 0 \\ 0 & 0 & k_n \end{bmatrix} \begin{Bmatrix} \Delta u \\ \Delta v \\ \Delta w \end{Bmatrix} \tag{13}$$

Substituting for $[B]$, $[C]$, and for the shape functions in the equation for $[k]$, and performing the integration, we will get the final stiffness matrix for the soil-reinforcement interface element as

$$[k_m] = \frac{1}{2} bL$$

$$\begin{bmatrix}
2k_{s1} & 0 & 0 & k_{s1} & 0 & 0 & -k_{s1} & 0 & 0 & -2k_{s1} & 0 & 0 \\
0 & 2k_{s2} & 0 & 0 & k_{s2} & 0 & 0 & -k_{s2} & 0 & 0 & -2k_{s2} & 0 \\
0 & 0 & 2k_n & 0 & 0 & k_n & 0 & 0 & -k_n & 0 & 0 & -2k_n \\
k_{s1} & 0 & 0 & 2k_{s1} & 0 & 0 & -2k_{s1} & 0 & 0 & -k_{s1} & 0 & 0 \\
0 & k_{s2} & 0 & 0 & 2k_{s2} & 0 & 0 & -2k_{s2} & 0 & 0 & -k_{s2} & 0 \\
0 & 0 & k_n & 0 & 0 & 2k_n & 0 & 0 & -2k_n & 0 & 0 & -k_n \\
-k_{s1} & 0 & 0 & -2k_{s1} & 0 & 0 & 2k_{s1} & 0 & 0 & k_{s1} & 0 & 0 \\
0 & -k_{s2} & 0 & 0 & -2k_{s2} & 0 & 0 & 2k_{s2} & 0 & 0 & k_{s2} & 0 \\
0 & 0 & -k_n & 0 & 0 & -2k_n & 0 & 0 & 2k_n & 0 & 0 & k_n \\
-2k_{s1} & 0 & 0 & -k_{s1} & 0 & 0 & k_{s1} & 0 & 0 & 2k_{s1} & 0 & 0 \\
0 & -2k_{s2} & 0 & 0 & -k_{s2} & 0 & 0 & k_{s2} & 0 & 0 & 2k_{s2} & 0 \\
0 & 0 & -2k_n & 0 & 0 & -k_n & 0 & 0 & k_n & 0 & 0 & 2k_n
\end{bmatrix} \tag{14}$$

After obtaining stiffness in the local x, y, and z coordinate system, it is transformed into the global X, Y, and Z coordinate system using a transformation matrix $[T']$

$$[T'] = \begin{bmatrix}
C_x & C_y & C_z \\
\dfrac{C_x C_z \sin\alpha - C_y \cos\alpha}{\sqrt{C_x^2 + C_y^2}} & \dfrac{C_x \cos\alpha + C_z C_y \sin\alpha}{\sqrt{C_x^2 + C_y^2}} & -\sqrt{C_x^2 + C_y^2}\sin\alpha \\
\dfrac{-C_y \sin\alpha - C_z C_x \cos\alpha}{\sqrt{C_x^2 + C_y^2}} & \dfrac{C_x \sin\alpha - C_z C_y \cos\alpha}{\sqrt{C_x^2 + C_y^2}} & \sqrt{C_x^2 + C_y^2}\cos\alpha
\end{bmatrix} \tag{15}$$

where

$$\sin\alpha = \frac{y_{k\gamma}}{\sqrt{y_{k\gamma}^2 + z_{k\gamma}^2}}, \quad \cos\alpha = \frac{z_{k\gamma}}{\sqrt{y_{k\gamma}^2 + z_{k\gamma}^2}} \tag{16}$$

$$x_{k\gamma} = C_x x_{ki} + C_y y_{ki} + C_z z_{ki} \tag{17}$$

$$y_{k\gamma} = \frac{-C_y}{\sqrt{C_x^2 + C_y^2}} x_{ki} + \frac{C_x}{\sqrt{C_x^2 + C_y^2}} y_{ki} \tag{18}$$

$$z_{k\gamma} = \frac{-C_z C_x}{\sqrt{C_x^2 + C_y^2}} x_{ki} - \frac{C_z C_y}{\sqrt{C_x^2 + C_y^2}} y_{ki} + \sqrt{C_x^2 + C_y^2}\, z_{ki} \tag{19}$$

$x_{ki} = x_k - x_i$, $y_{ki} = y_k - y_i$, $z_{ki} = z_k - z_i$, where x_k, y_k, and z_k = x, y, and z coordinates for the reference node k lying in the z-x plane in the local coordinate axes but not along the length of the member

$$C_x = (x_j - x_i)/L, \quad C_y = (y_j - y_i)/L, \quad C_z - (z_j - z_i)/L \tag{20a-c}$$

and

$$L = \sqrt{(x_j - x_i)^2 + (y_j - y_i)^2 + (z_j - z_i)^2} \tag{20d}$$

Here the rotation about the local x-axis is also considered so that the interface can be placed on the sides of the reinforcement if needed. The preceding transformation will not be valid for vertical interfaces where C_x and C_y will become zero (parallel to global Z-axis). In such a case $[T']$ can be obtained as

$$[T']_{ver} = \begin{bmatrix} 0 & 0 & C_z \\ C_z \sin\alpha & \cos\alpha & 0 \\ -C_z \cos\alpha & \sin\alpha & 0 \end{bmatrix} \tag{21}$$

where

$$\sin\alpha = \frac{y_{ki}}{\sqrt{x_{ki}^2 + y_{ki}^2}}, \quad \cos\alpha = \frac{-x_{ki}}{\sqrt{x_{ki}^2 + y_{ki}^2}} C_z \tag{22a,b}$$

The complete transformation matrix $[T]$ is obtained as

$$[T] = \begin{bmatrix} [T'] & 0 & 0 & 0 \\ 0 & [T'] & 0 & 0 \\ 0 & 0 & [T'] & 0 \\ 0 & 0 & 0 & [T'] \end{bmatrix} \tag{23}$$

and the global stiffness matrix as $[k] = [T]^T [k_m][T]$.

APPENDIX II. MATERIAL PROPERTIES

Soil Properties

Unit weight = 16.75×10^{-6} N/mm^3
Poisson's ratio = 0.3
Angle of internal friction = 38°
Coefficient of earth pressure at rest = 0.6
Hyperbolic constant K = 771
Hyperbolic constant n = 0.316
Hyperbolic constant R_f = 0.87
Cohesive strength = 0

Reinforcement Properties

Coir

E-value = 300 N/mm^2
Cross-sectional area = 14.75 mm^2
Poisson's ratio = 0.3

Bamboo

E-value = 18,000 N/mm^2
Cross-sectional area = 175 mm^2
Poisson's ratio = 0.3

Interface Properties

Steel and Sand (interface below the footing)

Angle of sliding friction = 22°
Hyperbolic constant K' = 38,580
Hyperbolic constant n' = 0.909
Hyperbolic constant R_f = 0.91

Coir and Sand

Angle of sliding friction = 42°
Hyperbolic constant K' = 10,231

Hyperbolic constant $n' = 0.4$
Hyperbolic constant $R_f' = 0.78$
Width of the interface $b = 4.3$ mm

Bamboo and Sand

Angle of sliding friction = 17.4°
Hyperbolic constant $K' = 17{,}018$
Hyperbolic constant $n' = 0.669$
Hyperbolic constant $R' = 0.848$
Width of interface $b = 35$ mm

APPENDIX III. REFERENCES

Akinmusura, J. O., and Akinbolade, J. A. (1981). "Stability of loaded footings on reinforced soil." *J. Geotech. Engrg.*, ASCE, 107(6), 819–827.

Ayyar, T. S. R., Joseph, J., and Beena, K. S. (1988). "Bearing capacity of sand reinforced with coir rope." *Proc., 1st Indian Geotextile Conf. on Reinforced Soil and Geotextiles*, A.11–16.

Beena, K. S. (1986). "Bearing capacity of sand reinforced with coir rope," M.Tech. thesis, Univ. of Kerala, India.

Beena, K. S. (1994). "Studies on the settlement of reinforced sand in foundations," PhD thesis, Indian Inst. of Technol., Madras, India.

Beer, G. (1985). "An isoparametric joint/interface element for finite element analysis." *Int. J. Numer. Methods in Engrg.*, 21(4), 585–600.

Binquet, J., and Lee, K. L. (1975). "Bearing capacity tests on reinforced earth soils." *J. Geotech. Engrg.*, ASCE, 101(12), 1241–1255.

Desai, C. S. (1974). "Numerical design-analysis of piles in sand." *J. Geotech. Engrg.*, ASCE, 100(6), 613–635.

Desai, C. S., and Abel, J. F. (1972). *Introduction to the finite element method.* Van Nostrand Reinhold, New York, N.Y.

Duncan, J. M., and Chang, C. Y. (1970). "Nonlinear analysis of stresses and strains in soils." *J. Soil Mech. and Found. Div.*, ASCE, 96(5), 1629–1653.

Fragaszy, R. J., and Lawton, E. (1984). "Bearing capacity of reinforced sand subgrades." *J. Geotech. Engrg.*, ASCE, 110(10), 1500–1511.

Gens, A., Carol, I., and Alonso, E. E. (1989). "An interface element formulation for the analysis of soil-reinforcement interaction." *Comp. and Geotech.*, 7, 133–151.

Ghaboussi, J., Wilson, E. L., and Isenberg, J. (1973). "Finite element for rock joints and interfaces." *J. Soil Mech. and Found. Div.*, ASCE, 99(10), 833–848.

Goodman, R. E., and St. John, C. (1977). "Finite element analysis for discontinuous rocks." *Numerical methods in geotechnical engineering*, C. S. Desai and J. T. Christian, eds., McGraw-Hill Inc., New York, N.Y., 148–175.

Goodman, R. E., Taylor, R. L., and Brekke, T. L. (1968). "A model for the mechanics of jointed rock." *J. Soil Mech. and Found. Div.*, ASCE, 94(3), 637–659.

Kinney, T. (1982). "Small scale load tests on a soil-geotextile-aggregate system." *Proc., 2nd Int. Conf. on Geotextiles*, 405–409.

Kondner, R. L., and Zelasko, J. S. (1963). "A hyperbolic stress-strain formulation for sands." *Proc., 2nd Pan Am. Conf. on Soil Mech. and Found. Engrg.*, 1, 289–324.

Kurian, N. P. (1992). *Design of foundation systems: principles and practices.* Addison-Wesley Publishing Co., Singapore, 64–67.

Lee, K. L. (1978). "Mechanism, analysis and design of reinforced earth, state-of-the art report." *Proc., Symp. on Earth Reinforcements*, ASCE, New York, N.Y., 62–76.

Muqtadir, A., and Desai, C. S. (1986). "Three-dimensional analysis of a pile-group foundation." *Int. J. Numer. and Analytical Methods in Geomech.*, 10, 41–58.

Nagoa, A., Kitamura, T., and Mizutani, J. (1988). "Field experiment on reinforced earth and its evaluation using FEM analysis." *Proc., Int. Geotech. Symp. on Theory and Practice of Earth Reinforcement*, 329–334.

Romstad, K. M., Herrmann, L. R., and Shen, C. K. (1976). "Integrated study of reinforced earth. I: Theoretical formulation." *J. Geotech. Engrg. Div.*, ASCE, 102(5), 457–471.

Singh, H. R. (1988). "Bearing capacity of reinforced soil beds," PhD thesis, Indian Inst. of Sci., Bangalore, India.

Vidal, H. (1969). "The principle of reinforced earth." *Hwy. Res. Rec. 282*, Washington, D.C.

Zienkiewicz, O. C. (1979). *The finite element method.* McGraw-Hill Inc., London, U.K.

APPENDIX IV. NOTATION

The following symbols are used in this paper:

a, b = Kondner's constants for soil;
a', b' = Kondner's constants for interfaces;
B = width of footing;
$[B]$ = strain-displacement matrix;
b = width of line interface;
$[C]$ = constitutive matrix;
C_x = uniformity coefficient;
C_x, C_y, C_z = direction cosines;
c = cohesive strength of soil;
D_{10} = effective size of soil particle;
E = Young's modulus;
E_i = initial tangent modulus;
E_t = tangent modulus;
e_{max} = maximum void ratio;
e_{min} = minimum void ratio;
$[F]$ = force vector;
G = specific gravity of soil;
K, n = hyperbolic constants for soil;
K', n' = hyperbolic constants for interfaces;
$[k]$ = stiffness matrix;
$[k_m]$ = element stiffness matrix in local direction;
k_n = interface normal stiffness in z-direction;
k_{st} = tangent shear stiffness;
k_{s1} = interface shear stiffness in x-direction;
k_{s2} = interface shear stiffness in y-direction;
L = length of element/reinforcement;
N_i = shape functions;
P_a = atmospheric pressure;
R_f = failure ratio for soil;
R_f' = failure ratio for interface;
s = horizontal spacing of reinforcement;
$[T]$ = transformation matrix;
$\{u\}$ = vector of displacement component;
u, v, w = nodal displacements in x, y, z-directions, respectively;
γw = unit weight of water;
Δu, Δv, Δw = relative displacements;
ε = axial strain;
σ_n = normal stress;
σ_1 = major principal stress;
σ_3 = minor principal stress;
τ = shear stress;
τ_x = shear traction (stress) along x-direction;
τ_y = shear traction (stress) along y-direction;
τ_{max} = asymptotic value of shear stress; and
ϕ = angle of internal friction of soil.

J. Geotech. Geoenviron. Eng. 1997.123:818-827.